Materials Research Proceedings 39 (2024) 32-41 https://doi.org/10.21741/9781644903094-5

Analytical Determination of the Geometrical Properties of Open-Celled Metal Foams Under Compression

Esmari Maré[1,a*] and Sonia Woudberg[1,b]

[1]Applied Mathematics Division, Department of Mathematical Sciences, Stellenbosch University, Private Bag X1, Matieland, Stellenbosch, 7602, Western Cape, South Africa

[a]esmari.mare@gmail.com, [b]fidder@sun.ac.za

Keywords: Metal Foams, Permeability, Specific Surface Area, Compression, Darcy, Forchheimer

Abstract. Several studies in the literature have been devoted to the permeability prediction of metal foams, including that involving the Representative Unit Cell (RUC) model. The RUC modelling approach is an attractive modelling method due to the simple rectangular geometry, as well as its satisfying performance in comparison to other models and experimental data as proven elsewhere in the literature for porous media. The subject of compression of metal foams has been addressed elsewhere in the literature, but this study is the first to involve an all-inclusive analytical model where both streamwise and transverse compression are accounted for. The Darcy and Forchheimer permeability coefficients of the compressed foam (or three-strut) RUC model are presented. Furthermore, a geometric approach requiring measured geometric parameters and a combined geometric-kinetic approach involving measured permeability coefficients are included for determining the specific surface area. Geometric parameters required to determine the permeability and specific surface area predictions using the compressed foam RUC model include the uncompressed porosity, pore dimension and strut diameter, as well as the compression factor. The model is evaluated through comparison with available experimental data and empirical models obtained from the literature for compressed metal foams. The compressed RUC model predictions produce expected tendencies of geometrical parameters of metal foams under compression and the comparison with experimental data reveal satisfactory results.

Introduction

In the literature the topic of compression of foamlike media is often addressed. [1] and [2], for example, mentioned the advantages of compressed metal foams in that with compression, the density of the foam increases and consequently improves heat transfer and structural rigidity. The only geometric model that accommodates the structural transformation induced by compression as found by the author in the literature, is the streamwise compression transformation of the three-strut Representative Unit Cell (RUC) model [3,4]. Compression in the transverse direction (i.e. perpendicular to the direction of flow) is another consideration since it does appear in experimental studies available in the literature. For example, [5] investigated the controlling of microfluidic flow in microphysiological systems by compressing foams. Other examples of studies regarding the compression of metal foams include [1], [6], [7] and [8]. In this study the foam (or three-strut) RUC model is adjusted to accommodate the accompanied structural transformations. The model presented retains the rectangular nature, but is adjusted to facilitate different pore dimensions for each of the three principal directions. The model can consequently be applied to streamwise or transverse compression by implementing structural assumptions to the adjusted RUC model presented. From the adjusted model, expressions for the Darcy permeability, Forchheimer permeability and specific surface area can be determined. The equations for the specific surface area obtained using a geometric approach (i.e. in terms of pore-scale dimensions) is included as well as an example of a combined geometric-kinetic approach where the measured permeability

coefficient is required, rather than one of the pore-scale dimensions, in order to determine the specific surface area. Finally, an example of how the structurally transformed RUC model is applied to a specific case study of compression is illustrated using available experimental data for the permeability coefficients and specific surface area.

Model parameters

In this study, permeability coefficients are defined such that they are related to the pressure drop, as described by the Darcy-Forchheimer equation, in the following manner:

$$\frac{\Delta p}{L} = \frac{\mu}{K} q + \frac{\rho}{K_F} q^2 \,, \tag{1}$$

where K and K_F are the permeability coefficients of the Darcy and Forchheimer regimes, respectively, $\Delta p/L$ is the pressure gradient, μ is the dynamic viscosity, ρ is the density of the fluid, and q is the superficial velocity. The compression factor, denoted by e_x, is introduced to relate the dimensions of the uncompressed models to the dimensions of the compressed models, where $0 < e_x \leq 1$. When $e_x = 1$, the pore dimension corresponds to the uncompressed state. The compression factor is given by the ratio $e_x = h_f/h_o$, where h_o and h_f respectively denote the uncompressed and post-compression thickness of the porous medium sample in question [9]. The compression factor in this study is consequently determined as follows:

$$e_x = \frac{d_x}{d_{x_o}} \,, \tag{2}$$

where d denotes the cell diameter of the RUC model and x respectively represents the subscripts '$\parallel$', '$\perp_1$' and '$\perp_2$' to denote compression in the streamwise direction and two possible transverse directions (e.g. $e_\parallel = d_\parallel/d_{\parallel_o}$ denotes the streamwise compression factor). The subscript 'o' denotes the uncompressed state. A general equation relating the porosity, ϵ, and compression factor was presented in [9,10], i.e.

$$\epsilon = 1 - \frac{1-\epsilon_o}{e_x} \,. \tag{3}$$

Eq. 3 is based on the assumption that the base area of the porous medium and the solid volume of the medium remains constant, as explained in [9]. In order to determine the values of the dimensions that are necessary to calculate the required predictions for the permeability coefficients and specific surface area provided by the adjusted RUC models, information regarding the direction of compression and compression factor are essential.

Adjusted three-strut RUC model

The three-strut RUC model with adjustable cell dimensions, is shown in Fig. 1. An expression for the porosity is determined first from which relations between the model dimensions can be obtained.

Materials Research Proceedings 39 (2024) 32-41 https://doi.org/10.21741/9781644903094-5

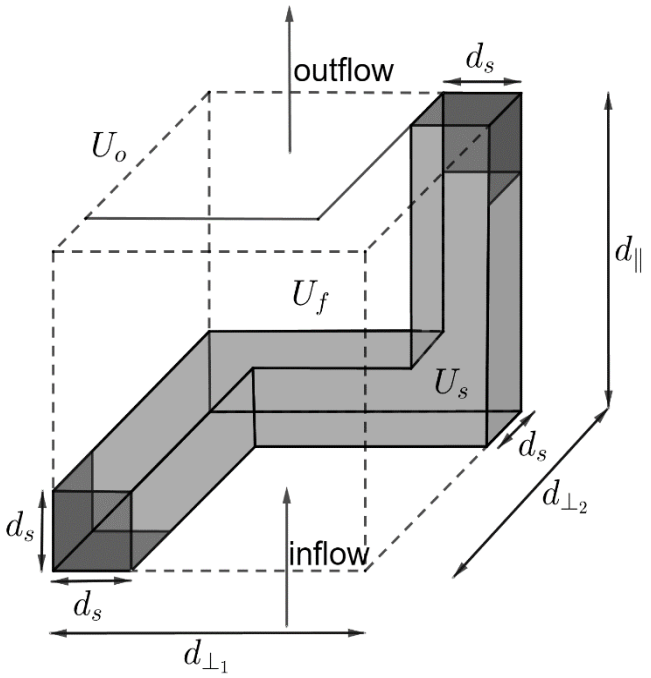

Fig. 1 Three-strut RUC model with adjustable dimensions

Model dimension relations. The total volume of the adjusted RUC model is $U_o = d_\parallel d_{\perp_1} d_{\perp_2}$ and the solid volume of the adjusted three-strut RUC model can be acquired from Fig. 1, which leads to the determination of the expression for the porosity, i.e.

$$\epsilon = 1 - \frac{U_s}{U_o} = 1 - \frac{{d_s}^2}{d_\parallel d_{\perp_1}} - \frac{{d_s}^2}{d_\parallel d_{\perp_2}} - \frac{{d_s}^2}{d_{\perp_1} d_{\perp_2}} + \frac{2\,{d_s}^3}{d_\parallel d_{\perp_1} d_{\perp_2}}. \tag{4}$$

Using Eq. 4, relations between the pore-scale dimensions and porosity can be attained.

Permeability prediction. In the studies of [3] and [10], an expression for the pressure drop of the Darcy flow regime is provided, as well as a derivation of the Darcy permeability coefficient of the RUC model. A similar pressure drop expression is provided in this study, with the difference that it is adapted to accommodate the adjustable dimensions of the adjusted three-strut RUC model, i.e.

$$\Delta p = \frac{S_{\parallel_1}\tau_{w_{\parallel_1}} + S_{\parallel_2}\tau_{w_{\parallel_2}} + S_{\perp_{1,1}}\tau_{w_{\perp_{1,1}}} + S_{\perp_{1,2}}\tau_{w_{\perp_{1,2}}} + S_{\perp_{2,1}}\tau_{w_{\perp_{2,1}}} + S_{\perp_{2,2}}\tau_{w_{\perp_{2,2}}}}{A_{p_\parallel}}. \tag{5}$$

In Eq. 5, $S_\parallel$, $S_{\perp_1}$ and $S_{\perp_2}$ denote the surface areas oriented in the directions relative to flow (which includes two transverse directions) and $\tau_\parallel$, $\tau_{\perp_1}$ and $\tau_{\perp_2}$ denote the magnitude of the corresponding average wall shear stresses. The subscripts of '1' and '2' in Eq. 5 (the second numerical subscript in the case of the transverse parameters) are utilized in order to distinguish between the two surface areas bounding the same channel as well as the magnitude of the corresponding average wall shear stresses. Using Fig. 1, the surface areas and average wall shear stress expressions are consequently determined to be

$$S_{\parallel_1} = 2d_s\left(d_{\perp_1} - d_s\right), \tag{6}$$
$$S_{\parallel_2} = 2d_s\left(d_{\perp_2} - d_s\right), \tag{7}$$

$$S_{\perp_{1,1}} = 2d_s\left(d_{\perp_2} - d_s\right), \tag{8}$$
$$S_{\perp_{1,2}} = 2d_s(d_{\parallel} - d_s), \tag{9}$$
$$S_{\perp_{2,1}} = 2d_s\left(d_{\perp_1} - d_s\right), \tag{10}$$
$$S_{\perp_{2,2}} = 2d_s(d_{\parallel} - d_s), \tag{11}$$

and

$$\tau_{w_{\parallel_1}} = \frac{6\mu w_{\parallel}}{d_{\perp_2} - d_s} = \frac{6d_{\perp_1}d_{\perp_2}}{(d_{\perp_1} - d_s)(d_{\perp_2} - d_s)^2}\,\mu q, \tag{12}$$
$$\tau_{w_{\parallel_2}} = \frac{6\mu w_{\parallel}}{d_{\perp_1} - d_s} = \frac{6d_{\perp_1}d_{\perp_2}}{(d_{\perp_1} - d_s)^2(d_{\perp_2} - d_s)}\,\mu q, \tag{13}$$
$$\tau_{w_{\perp_{1,1}}} = \frac{6\mu w_{\perp_1}}{d_{\parallel} - d_s} = \frac{6d_{\perp_1}d_{\perp_2}}{(d_{\parallel} - d_s)^2(d_{\perp_2} - d_s)}\,\mu q, \tag{14}$$
$$\tau_{w_{\perp_{1,2}}} = \frac{6\mu w_{\perp_1}}{d_{\perp_2} - d_s} = \frac{6d_{\perp_1}d_{\perp_2}}{(d_{\parallel} - d_s)(d_{\perp_2} - d_s)^2}\,\mu q, \tag{15}$$
$$\tau_{w_{\perp_{2,1}}} = \frac{6\mu w_{\perp_2}}{d_{\parallel} - d_s} = \frac{6d_{\perp_1}d_{\perp_2}}{(d_{\parallel} - d_s)^2(d_{\perp_1} - d_s)}\,\mu q, \tag{16}$$
$$\tau_{w_{\perp_{2,2}}} = \frac{6\mu w_{\perp_2}}{d_{\perp_1} - d_s} = \frac{6d_{\perp_1}d_{\perp_2}}{(d_{\parallel} - d_s)(d_{\perp_1} - d_s)^2}\,\mu q, \tag{17}$$

respectively. $w_{\parallel}$, $w_{\perp_1}$ and $w_{\perp_2}$ in Eqs. 12 to 17 denote the average channel velocities in the indicated directions. The expression for the streamwise cross-sectional flow area ($A_{p_{\parallel}}$) is furthermore given by

$$A_{p_{\parallel}} = \left(d_{\perp_1} - d_s\right)\left(d_{\perp_2} - d_s\right). \tag{18}$$

Substituting the equations for the surface areas as given by Eqs. 6 to 11, Eqs. 12 to 17 and Eq. 18 into Eq. 5, leads to the following equation for the pressure gradient of the Darcy flow regime:

$$\frac{\triangle p}{d_{\parallel}} = \frac{24\,d_s\,d_{\perp_1}d_{\perp_2}\mu q}{d_{\parallel}(d_{\perp_1} - d_s)(d_{\perp_2} - d_s)}\left[\frac{1}{(d_{\parallel} - d_s)^2} + \frac{1}{(d_{\perp_1} - d_s)^2} + \frac{1}{(d_{\perp_2} - d_s)^2}\right]. \tag{19}$$

The equation used to determine the pressure gradient of the Forchheimer flow regime is the same as the equation utilized for this purpose by [11], i.e.

$$-\nabla\langle p\rangle_f = \frac{S_{\text{face}}}{\epsilon U_o}\rho {w_{\parallel}}^2\underline{\hat{n}} = \frac{d_{\perp_1}d_{\perp_2}(d_s d_{\perp_1} - {d_s}^2)}{\epsilon d_{\parallel}(d_{\perp_1} - d_s)^2(d_{\perp_2} - d_s)^2}\,\rho q^2\underline{\hat{n}}, \tag{20}$$

where S_{face} is the cross-sectional solid area that faces upstream, as determined from Fig. 1. The Ergun-type equation consequently leads to

$$\frac{\triangle p}{d_{\parallel}} = \frac{24\,d_s\,d_{\perp_1}d_{\perp_2}}{d_{\parallel}(d_{\perp_1} - d_s)(d_{\perp_2} - d_s)}\left[\frac{1}{(d_{\parallel} - d_s)^2} + \frac{1}{(d_{\perp_1} - d_s)^2} + \frac{1}{(d_{\perp_2} - d_s)^2}\right]\mu q + \frac{d_{\perp_1}d_{\perp_2}(d_s d_{\perp_1} - {d_s}^2)}{\epsilon d_{\parallel}(d_{\perp_1} - d_s)^2(d_{\perp_2} - d_s)^2}\,\rho q^2, \tag{21}$$

and comparing Eq. 21 with Eq. 1 yields the expressions of the Darcy and Forchheimer permeability coefficients of the adjusted three-strut RUC model, respectively denoted by K and K_F, i.e.

$$K = \frac{d_{\parallel}(d_{\perp_1} - d_s)(d_{\perp_2} - d_s)}{24\, d_s\, d_{\perp_1} d_{\perp_2}} \left[\frac{1}{(d_{\parallel} - d_s)^2} + \frac{1}{(d_{\perp_1} - d_s)^2} + \frac{1}{(d_{\perp_2} - d_s)^2} \right]^{-1}, \tag{22}$$

and

$$K_F = \frac{\epsilon d_{\parallel}(d_{\perp_1} - d_s)^2 (d_{\perp_2} - d_s)^2}{d_{\perp_1} d_{\perp_2} (d_s d_{\perp_1} - {d_s}^2)}. \tag{23}$$

Specific surface area: geometric approach. The total surface area of the adjusted three-strut RUC model can be determined by adding all the individual surface areas given by Eqs. 6 to 11. Dividing the result by the total RUC volume, the equation for the specific surface area can be determined, i.e.

$$S_v = \frac{4\, d_s}{d_{\parallel} d_{\perp_1} d_{\perp_2}} \left[(d_{\parallel} - d_s) + (d_{\perp_1} - d_s) + (d_{\perp_2} - d_s) \right]. \tag{24}$$

Due to the dependence of the specific surface area on the geometry of the three-strut RUC model as shown in Fig. 1, the porosity equation (Eq. 4) relates the dimensions in Eq. 24.

Specific surface area: combined approach. In the combined kinetic-geometric approach for determining the specific surface area, also referred to as simply the combined approach, a permeability coefficient is utilized to determine S_v instead of one of the pore-scale dimensions. Either one of the pore-scale dimensions in Eq. 24 can be replaced. The substitution of an expression for K instead of the pore-scale dimension $d_{\parallel}$ is considered in this study as an example of acquiring the specific surface area using a combined approach. First, the expression for S_v (i.e. Eq. 24), needs to be rearranged to determine $d_{\parallel}$ in terms of the specific surface area. This yields

$$d_{\parallel} = \frac{4s - 4{d_s}^2}{d_{\perp_1} d_{\perp_2} S_v - 4 d_s}, \tag{25}$$

where $s = d_s\left[(d_{\perp_1} - d_s) + (d_{\perp_2} - d_s)\right]$. Eq. 25 is then substituted into Eq. 19 and rearranged in order to obtain the following third degree polynomial in S_v from which S_v can be solved:

$$a'\, {S_v}^3 + b'\, {S_v}^2 + c'\, S_v + g' = 0,$$

where

$$\begin{aligned}
a' &= -K {d_{\perp_1}}^3 {d_{\perp_2}}^3 (1 + n {d_s}^2) \\
b' &= 12 K d_s\, {d_{\perp_1}}^2 {d_{\perp_2}}^2 (1 + n {d_s}^2) + 4 d_s {d_{\perp_1}}^2 {d_{\perp_2}}^2 (m d_s + 2nK)(s - {d_s}^2) \\
c' &= -48 K {d_s}^2 d_{\perp_1} d_{\perp_2} (1 + n {d_s}^2) - 32 {d_s}^2 d_{\perp_1} d_{\perp_2} (m d_s + 2nK)(s - {d_s}^2) \\
&\quad - 16 d_{\perp_1} d_{\perp_2} (2 m d_s + nK)(s - {d_s}^2)^2 \\
g' &= 64 K {d_s}^3 (1 + n {d_s}^2) + 64 {d_s}^3 (m d_s + 2nK)(s - {d_s}^2) + 64 d_s (2 m d_s + nK)(s - {d_s}^2)^2 \\
&\quad + 64 m (s - {d_s}^2)^3.
\end{aligned} \tag{26}$$

with $m = \frac{(d_{\perp_1} - d_s)(d_{\perp_2} - d_s)}{24\, d_s\, d_{\perp_1} d_{\perp_2}}$ and $n = \frac{1}{(d_{\perp_1} - d_s)^2} + \frac{1}{(d_{\perp_2} - d_s)^2}$. It should be noted that in order to determine the specific surface area by making use of the combined approach, experimental permeability data is required, e.g. experimental Darcy permeability data should be substituted into

Eq. 26 in order to determine the specific surface area of the adjusted three-strut RUC model when using Eq. 26.

Model application and validation

In this section, the manner in which the compressed three-strut RUC model can be utilized and validated, using available experimental data obtained from [12], is shown and the predictions acquired are compared to that of the corresponding uncompressed model and experimental data. [12] investigated the correlations of the pressure drop for air flow through different foam samples, of which some were compressed. Permeability and specific surface area data for four of these foam samples that were compressed in the streamwise direction are shown in Table 1.

Table 1 Experimental data obtained from [12] for aluminum foams

ϵ_o [ ]	ϵ [ ]	e [ ]	$d_{p_o}[\mu\mathrm{m}]$	$K \times 10^9[\mathrm{m}^2]$	$K_F \times 10^3[\mathrm{m}]$	S_v $[\mathrm{m}^{-1}]$
0.921	0.679	0.246	1300	0.66	0.323	5104.3
0.921	0.774	0.350	1300	0.10	0.500	3593.7
0.922	0.682	0.245	2500	0.10	0.588	3169.3
0.922	0.794	0.379	2500	0.21	0.00012	2053.1

The uncompressed porosity and PPI numbers (and hence a way to obtain the uncompressed pore diameter) were provided by [12], along with corresponding porosity and compression factor data, as shown in Table 1. The compression factor data, however, was determined by [12] by using Eq. 3 which assumes no lateral expansion of the foam under compression, as mentioned in the model parameters section of this study. Consequently, this condition is assumed in this study. Due to the media samples being compressed in the streamwise direction, it is deduced from Eq. 2 that

$$d_{\parallel} = e_{\parallel} d_{\parallel_o} . \tag{27}$$

No value for the uncompressed strut diameter d_{s_o} or the uncompressed cell diameter $d_{\parallel_o}$ was provided by [12] from which all the parameters associated with the uncompressed state can be determined. Therefore, it is assumed that the uncompressed state of the three-strut RUC model is isotropic. This is similar to the assumption made by [13] in the implementation of the streamwise compressed three-strut RUC model in the application to data provided by [14]. Consequently, $d_{\parallel_o} = d_{\perp_{1_o}} = d_{\perp_{2_o}} = d_o$ and d_o can be obtained using the following relations between the dimensions of the isotropic three-strut RUC model:

$$d_o = \frac{2 d_{p_o}}{3 - \psi_o}, \tag{28}$$

where $d_{s_o} = d_o - d_{p_o}$ and ψ_o denoted a geometric factor, given by [3]

$$\psi_o = 2 + 2\cos\left[\frac{4\pi}{3} + \frac{1}{3}\cos^{-1}(2\epsilon_o - 1)\right]. \tag{29}$$

It is furthermore assumed that $d_{\perp_1} = d_{\perp_2} = d_o$, due to no lateral expansion. Due to the decrease in porosity combined with the assumption of constant solid volume during compression, as well as the condition of no lateral expansion, d_s increases with compression. The value of d_s can be determined from the following rearrangement of Eq. 4:

Materials Research Proceedings 39 (2024) 32-41 https://doi.org/10.21741/9781644903094-5

$$2{d_s}^3 + (-2d_o - d_\parallel){d_s}^2 + {d_o}^2 d_\parallel (1-\epsilon) = 0\,. \tag{30}$$

The Darcy permeability coefficient, Forchheimer permeability coefficient and specific surface area obtained using the geometric approach are thus, respectively, given by

$$K = \frac{d_\parallel (d_o - d_s)^2}{24 d_s {d_o}^2}\left[\frac{1}{(d_\parallel - d_s)^2} + \frac{2}{(d_o - d_s)^2}\right]^{-1}, \tag{31}$$

$$K_F = \frac{\epsilon d_\parallel (d_o - d_s)^3}{2 d_s {d_o}^2}, \tag{32}$$

and

$$S_v = \frac{4 d_s}{d_\parallel {d_o}^2}[(d_\parallel - d_s) + 2(d_o - d_s)]\,. \tag{33}$$

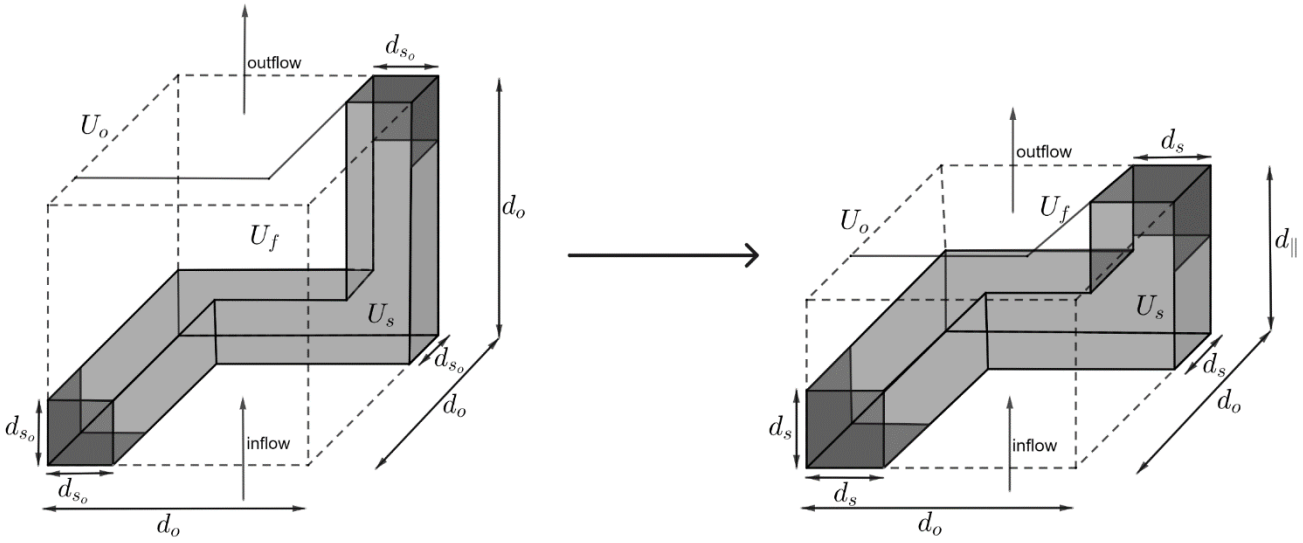

Fig. 2 Three-strut RUC model under streamwise compression without lateral expansion

The combined approach for determining the specific surface area can be utilized due to the availability of both permeability and specific surface area data by replacing $d_\parallel$ with K. A visual representation of the streamwise compressed three-strut RUC model subject to deformation (with no lateral expansion) is shown in Fig. 2. In Figs. 3 to 5 the predictions and experimental data of the Darcy permeability coefficient, Forchheimer permeability coefficient and specific surface area (using both the geometric and combined approach of attaining S_v), utilizing the data provided in Table 1 together with Eqs. 27 to 33, are shown, respectively. Empirical expressions for the Darcy permeability and form drag coefficients were furthermore provided by [2] and [12], from which the expression for the form drag coefficient can be utilized to obtain the prediction for the Forchheimer permeability coefficient. The permeability predictions acquired and corresponding data for the foam samples of [12] are included in Figs. 3 and 4. In Fig. 3 the compressed three-strut RUC model predictions provide closer correspondence to the experimental data than the uncompressed model predictions and In Fig. 4 it can be seen that the compressed RUC model corresponds excellently with the experimental data and performs better than the uncompressed and empirical models considered. The values provided by the experimental data are lower than that of the uncompressed model for both permeability coefficients, as expected, with the compressed three-strut RUC model predictions being in turn lower than that of the uncompressed model predictions. It is also noted that the compressed three-strut RUC model also provides closer

Materials Research Proceedings 39 (2024) 32-41 https://doi.org/10.21741/9781644903094-5

predictions to the experimental data than that of the empirical models of [2] and [10], which lends favor to the adjusted foam RUC model presented in this study.

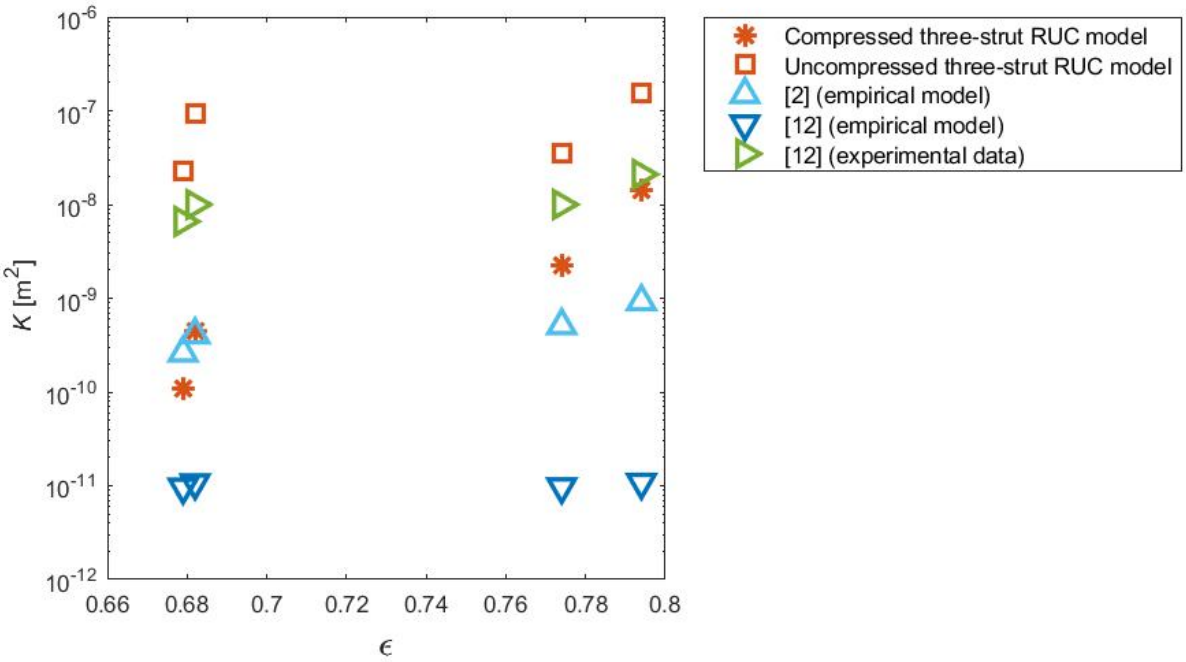

Fig. 3 Darcy permeability prediction versus porosity of RUC models and metal foam experimental data obtained from [10] under compression

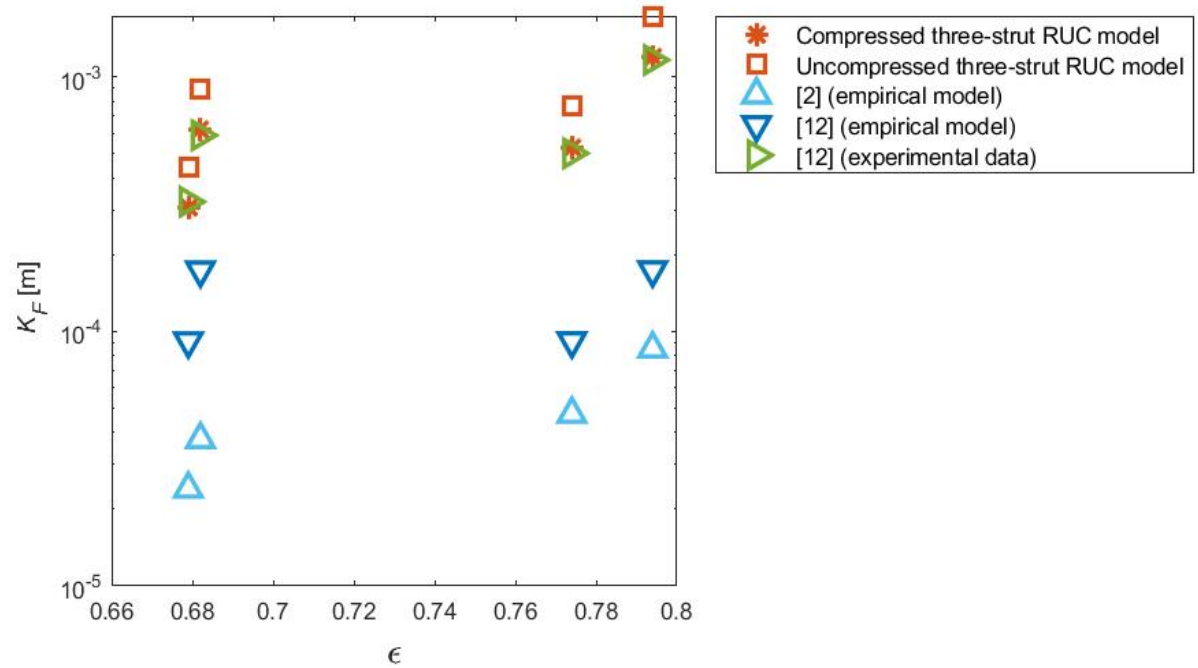

Fig. 4 Forchheimer permeability prediction versus porosity of RUC models and metal foam experimental data obtained from [10] under compression

Materials Research Proceedings 39 (2024) 32-41 https://doi.org/10.21741/9781644903094-5

In Fig. 5 the compressed three-strut RUC model once again corresponds closer to the experimental data, resulting from the predictions obtained using a geometric approach. The specific surface area predictions of the compressed RUC model acquired using a combined approach, however, corresponds closer to the predictions of the uncompressed model, which significantly under predicts the data. This may be due to the uncertainty already incorporated into the permeability prediction which is used as input to the combined approach. The combined approach can however be used to obtain S_v values of the correct order of magnitude, should specific surface area data be required but is unavailable.

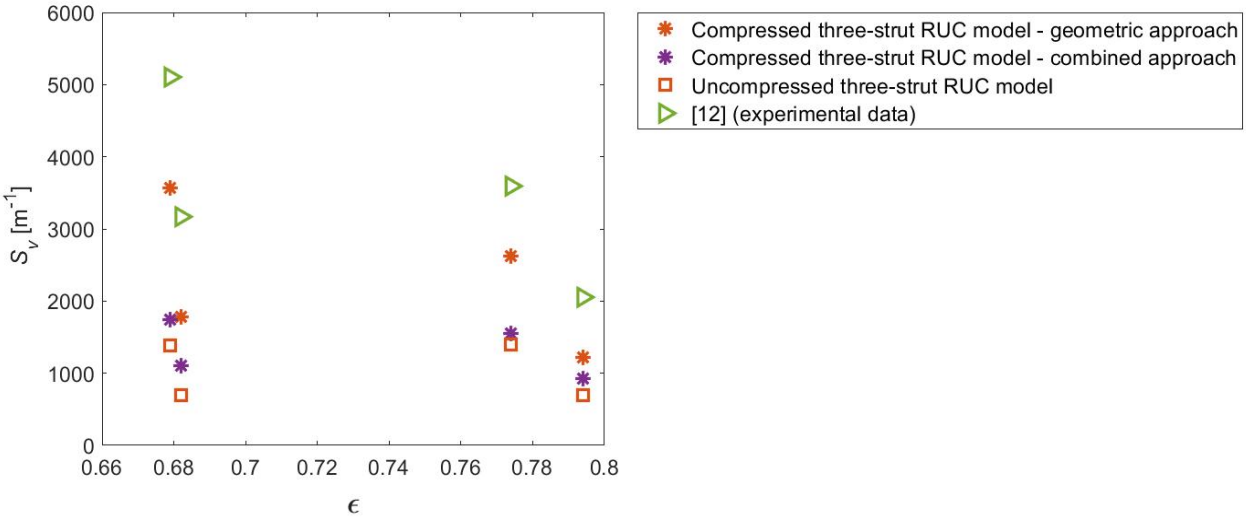

Fig. 5 Specific surface area prediction versus porosity of RUC models and metal foam experimental data obtained from [10] under compression

Summary

An adjusted foam (or three-strut) RUC model was presented that accommodates the parameter adjustments associated with compressed foamlike media and can be utilized in the application of both streamwise and transverse compression. Predictions for the Darcy and Forchheimer permeability coefficients, based on the adjusted three-strut RUC model, have been proposed, as well as the specific surface area prediction in terms of the linear pore-scale dimensions of the foam. A combined method for obtaining the specific surface area using the Darcy permeability, was furthermore included, where the experimentally obtained permeability can be utilized instead of one of the pore-scale dimensions, should specific surface area values be required and data is unavailable. Validation of the compressed RUC model was presented for streamwise compression with no lateral expansion and demonstrated using available experimental data. Comparison with experimental data for compressed foams revealed that the compressed model shows an improvement in predictions for the Darcy and Forchheimer coefficient values as well as specific surface area predictions when compared to that of the uncompressed model. Further model validation can be supported through the availability of additional experimental data that include measured characteristics of the uncompressed foam (i.e. the strut diameter of the uncompressed state) as well as permeability and specific surface area values of the compressed foam.

References

[1] B.V. Antohe, J.L. Lage, D.C. Price, R.M. Weber, Experimental determination of permeability and inertia coefficients of mechanically compressed aluminum porous matrices, ASME. J. Fluids Eng. Vol. 119(2) (1997) 404-412. https://doi.org/10.1115/1.2819148

[2] N. Dukhan, R. Picón-Feliciano, Á.R. Álvarez-Hernández, Air flow through compressed and uncompressed aluminum foam: measurements and correlations, ASME. J. Fluids Eng. 128(5) (2006) 1004-1012. https://doi.org/10.1115/1.2236132

[3] S. Woudberg, M.C. van Heyningen, L. Le Coq, J. Legrand, J.P. Du Plessis, Analytical determination of the effect of compression on the permeability of fibrous porous media, Chem. Eng. Sci. 112 (2014) 108-115. https://doi.org/10.1016/j.ces.2014.03.013

[4] S. Woudberg, E. Maré, M.C. van Heyningen, F. Theron, L. Le Coq, Predicting the permeability and specific surface area of compressed and uncompressed fibrous media including the Klinkenberg effect, Powder Technol. 377 (2021) 488-505. https://doi.org/10.1016/j.powtec.2020.08.081.

[5] S. Hong, Y. Jung, R. Yen, H.F. Chan, K.W. Leong, G.A. Truskey, X. Zhao, Magnetoactive sponges for dynamic control of microfluidic flow patters in microphysiological systems, Lab Chip 14(3) (2014) 514-521. http://dx.doi.org/10.1039/C3LC51076J

[6] K. Boomsma, D. Poulikakos, The effects of compression and pore size variations on the liquid flow characteristics in metal foams, ASME. J. Fluids Eng. 124(1) (2002) 263-272. https://doi.org/10.1115/1.1429637

[7] J. Hwang, G. Hwang, R. Yeh, C. Chao, Measurement of interstitial convective heat transfer and frictional drag for flow across metal foams, ASME. J. Heat Transfer 124(1) 120-129. http://doi.org/10.1115/1.1416690

[8] M.A. Dawson, J.T. Germaine, L.J. Gibson, Permeability of open-cell foams under compressive strain, Int J. Solids Struct. 44(16) (2007) 5133-5145. https://doi.org/10.1016/j.ijsolstr.2006.12.025

[9] M.C. van Heyningen, Investigating the effect of compression on the permeability of fibrous porous media, MSc Thesis, Stellenbosch University, South Africa, 2014.

[10] S. Woudberg, Permeability prediction of an analytical pore-scale model for layered and isotropic fibrous porous media, Chem. Eng. Sci. 164 (2017) 232-245. https://doi.org/10.1016/j.ces.2017.01.061

[11] S. Woudberg, J.P. Du Plessis, An analytical Ergun-type equation for porous foams, Chem. Eng. Sci. 148 (2016) 44-54. https://doi.org/10.1016/j.ces.2016.03.013

[12] N. Dukhan, Correlations for the pressure drop for flow through metal foam, Exp Fluids 41 (2006) 665-672. https://doi.org/10.1007/s00348-006-0194-x

[13] S. Woudberg, Investigation of the effect of compression on a soft fibrous porous medium, Computational Methods in Multiphase Flow VII 79, 2013, pp.351.

[14] H.D. Akaydin, A. Pierides, S. Weinbaum, Y. Andreopoulos, Permeability of soft porous media under one-dimensional compaction, Chem. Eng. Sci. 66(1) (2011) 1-14. https://doi.org/10.1016/j.ces.2010.09.017